Molecular Recognition

DOI: 10.1002/ange.200603807

Functional Architecture of HCV IRES Domain II Stabilized by Divalent Metal Ions in the Crystal and in Solution**

*Sergey M. Dibrov, Hillary Johnston-Cox, Yi-Hsin Weng, and Thomas Hermann**

The RNA genome of the hepatitis C virus (HCV) contains an internal ribosome entry site (IRES), which binds to the host-cell 40S ribosomal subunit and initiates protein translation in the absence of most initiation factors.[1,2] Recruitment of the ribosomal subunit to the HCV RNA is driven by the high affinity of the IRES–40S interaction.[3] The IRES sequence adopts a highly ordered secondary structure (Figure 1 a).[4] The three-dimensional architecture of the IRES is dominated by independently folding RNA domains.[5] Structures of IRES–40S complexes have been studied by cryo-electron microscopy (cryo-EM) revealing the overall shape of the RNA.[6,7] Higher-resolution structures of individual subdomains, including II[8] and IIIa–e,[9–12] have been determined by crystallography and NMR spectroscopy. Cryo-EM studies revealed that the domain II, which plays an important structural role in HCV translation,[13] adopts an L-shaped conformation that directs the apical hairpin loop IIb to overlap with the ribosomal E site in the proximity of the P site.[6] Binding of domain II induces a conformational change in the 40S head[7] and closes the messenger RNA (mRNA) binding cleft.[6] NMR studies suggested that subdomain IIa might be a flexible hinge whose bent state is stabilized by binding of divalent metal ions.[8]

To investigate the molecular architecture of the IRES domain II kink and its metal-ion-dependent stabilization, we have used X-ray crystallography and structure-guided incorporation of fluorescent labels. For X-ray crystal structure determination (see Figure S4 and Table S1 in the Supporting Information), an oligonucleotide (IIa-1) was used that contained residues 49–69 and 100–115 of the HCV IRES (Figure 1). The overall structure of the RNA revealed a bent architecture for the IIa subdomain. The two stems that are flanking the internal bulge are arranged at a right angle (Figure 1 b).[14]

The upper stem (residues 58–69/100–110) forms a continuous helix that contains both standard and noncanonical base pairs that adopt *cis*-Watson–Crick geometries. U106 is looped out from the stem to allow continuous stacking of the flanking base pairs. The arrangement of residues of the internal bulge introduces a right-angled bend in the RNA

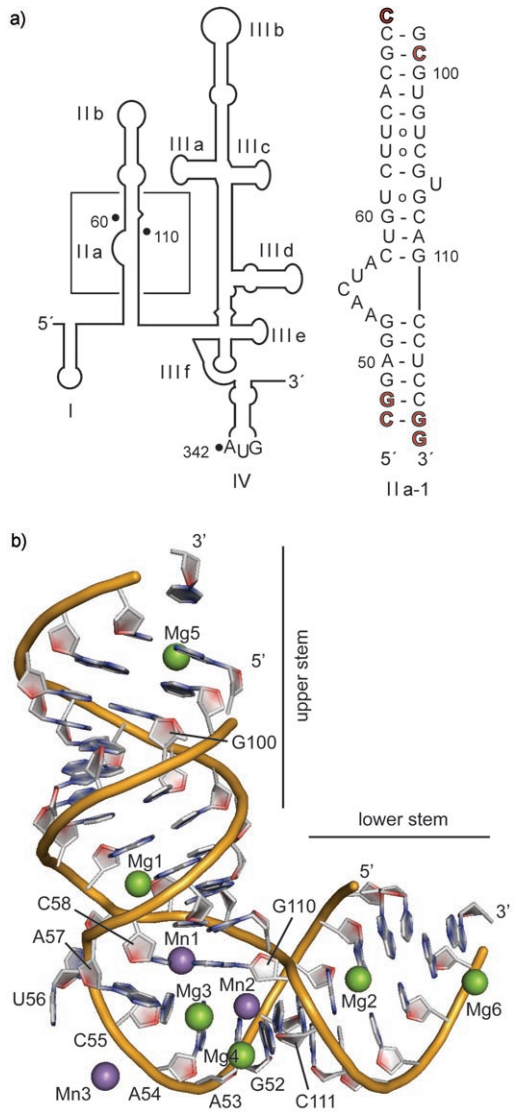

Figure 1. a) Secondary structure of the HCV 5′-nontranslated region that contains the IRES element and the subdomain IIa-1 construct used for crystallization and fluorescence labeling. The position of the IIa-1 construct within the IRES is indicated by a box. The nucleotides shown in red were changed in the construct from the HCV (genotype 1b) sequence to improve RNA stability. Non-Watson–Crick base pairs are indicated by "o" symbols. The numbering scheme for the construct has been adopted from the full HCV RNA. b) The three-dimensional structure of the IIa-1 RNA. Positions of metal ions are shown as spheres (Mg^{2+} green; Mn^{2+} magenta).

[*] Dr. S. M. Dibrov, H. Johnston-Cox, Y.-H. Weng, Dr. T. Hermann
Department of Chemistry and Biochemistry
University of California, San Diego
9500 Gilman Drive, La Jolla, CA 92093 (USA)
Fax: (+1) 858-534-0202
E-mail: tch@ucsd.edu

[**] We thank N. Nguyen for assistance with crystallographic data collection, Dr. C. Kim for help with data processing, and J. Parsons for help with UV melting experiments. This work was supported by faculty startup funds from the University of California, San Diego.
HCV = hepatitis C virus, IRES = internal ribosome entry site.

Supporting information for this article is available on the WWW under http://www.angewandte.org or from the author.

between the base pairs G52–C111 and C58–G110 that is stabilized by a combination of base stacking, hydrogen bonding, and metal-ion participation (see Figure 2 and Figure S5 in the Supporting Information). The bases of A53, A54, and C55 extend the lower stem into the bend by continuously stacking on the G52–C111 pair. A57 is oriented perpendicular to C55 and stacks on C58 in an extension of the upper stem. The connecting residue U56 is looped out from the RNA with the uridine base packed against the ribose of A57. NMR spectroscopic studies suggest that, in solution, different conformations may exist for U56.[8]

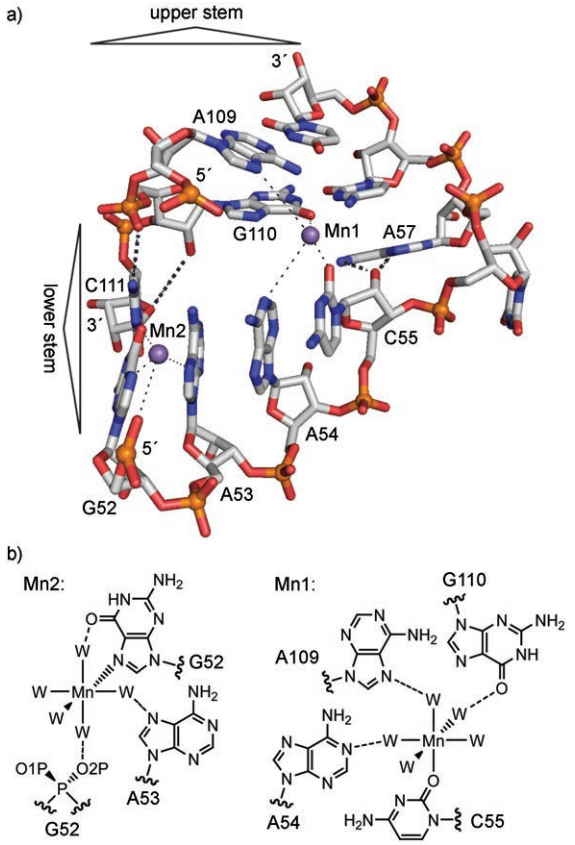

Figure 2. a) Hydrogen-bonding network and metal-ion binding in the IRES subdomain IIa internal bulge. The metal-ion sites Mn1 and Mn2 are 10 Å apart. The view of the bulge is rotated by 180° relative to Figure 1. b) Interactions of two Mn^{2+} ions bound at the internal bulge. Direct coordination (≈2.3–2.4 Å distance) is observed for Mn1···O2-(C55) and Mn2···N7(G52). Both metal ions are involved in three additional water-mediated contacts to the RNA (≈3.8–4.4 Å distance of Mn^{2+} to N or O; see Table S2 in the Supporting Information). Water molecules are indicated as W.

The perpendicular arrangement of base pairs G52–C111 and C58–G110 is locked in place by two metal ions and four hydrogen bonds. A right-angled kink in the backbone between residues C55 and A57 is stabilized by interaction of the 2′-OH group of C55 with both the N6 amino group and N7 atom of the A57 Hoogsteen edge (Figure 2a). In the other strand, the 90° angle between the bases of G110 and C111 is arrested by hydrogen bonds between the N4 amino group of C111 and the G110 phosphate group as well as the O4′ atom of C111 and the G111 2′-OH group.

The overall bend in the IIa subdomain has also been observed in the NMR spectroscopic structure.[8] The predominance of the bent architecture of subdomain IIa RNA both in the crystal and in solution indicate that, in the presence of divalent metal ions, the internal bulge constitutes a highly stable structural motif.

Two essential structural features of the IIa subdomain, the bend at the internal bulge, and the looped-out residue U106 are stabilized by divalent metal ions.[15] In the crystal, two Mn^{2+} ions, which can replace Mg^{2+},[16] were bound at the internal bulge, each forming at least one direct interaction with the RNA strand (Figure 2). The binding site Mn1 organizes the RNA structure at the center of the bend by providing an anchor at the interface of the upper and lower stems. Consecutive residues A54 and C55 in the lower stem as well as A109 and G110 in the upper stem are pulled together by the cation Mn1 in a perpendicular orientation. Additional stabilization is provided by the metal site Mn2, which locks A53 in place as a stacking platform for A54 and C55. Thus, what would be a conformationally labile stack of single-stranded residues (A53–C55) is rigidified by metal ions bound at Mn1 and Mn2.

In the upper stem, a Mg^{2+} ion at site Mg1 (Figure 1b and Table S2 in the Supporting Information) facilitates looping out of U106, which in turn allows continuous stacking of the flanking base pairs G105–C62 and G107–U61. The expulsion of U106 from the double helix leads to rotation of the G107 phosphate group, which, by interaction with Mg1, is locked facing the inside of the RNA major groove (see Figure S6 in the Supporting Information). A second Mg^{2+} ion, Mg2, is found at the Hoogsteen edge of a guanine (G49), a well-known binding site for divalent cations.[17,18]

The crystal structure suggests that metal-ion binding sites are key to the bent functional architecture of the IRES subdomain IIa. We next investigated the interaction of the RNA molecule with metal ions in solution by using UV absorption spectroscopy and fluorescent labeling. Thermal denaturation curves[19] of the double-stranded construct IIa-1 in the absence and presence of metal ions (see Figure S7 in the Supporting Information) show that the stability of the RNA was greatly increased in the presence of Mg^{2+}, suggesting tight binding of cations at specific sites that contribute to stabilization of the RNA fold. In contrast, monovalent K^+, even at a 10-fold-higher concentration, caused only a small shift in the denaturation curve, in agreement with general stabilization of the RNA by diffusely bound cations.[16]

Introduction of the fluorescent base analogue 2-aminopurine (2AP)[20–22] allowed us to monitor and quantify binding of cations in solution. Our rationale for the experiments was that metal-induced structure formation in the IIa-1 RNA would lead to changes in the fluorescent state of the 2AP label. Hence, quantification of fluorescence curves recorded over titrations with metal ions would allow us to determine cation binding affinities.

Based on their proximity to the key metal site, Mn1 (Figure 2a) and residues A54 and A57 were chosen for

replacement with 2AP. The crystal structure of IIa-1 suggested that neither substitution would interfere with metal binding at Mn1 or correct folding of the RNA. Replacement of adenine with 2AP at position 57, however, will disrupt one of the hydrogen bonds to the 2′-OH group of C55 (Figure 2a). We assumed that the 2AP57-labeled IIa-1 RNA would still adopt the native architecture as the second hydrogen bond of 2′-OH(C55) to N7(2AP57) is not affected by the 2AP substitution.

During titration of 2AP-labeled IIa-1 RNA with manganese or magnesium salt, dose-dependent quenching of fluorescence was observed for both the 2AP54 and 2AP57 constructs. Addition of Mg^{2+} led to fluorescence reduction of approximately 30% over the range of the titration (1 nM–100 mM), whereas Mn^{2+} quenched fluorescence by approximately 50%. In contrast, titrations with monovalent salt did not induce significant changes in the fluorescence (Figure S8 in the Supporting Information). These findings suggest that the fluorescent labels at positions 54 and 57 indeed report on specific binding of divalent cations at the nearby sites Mn1 and Mn2.

Fitting the titration data with binding curves for one-site or two-site binding models allowed calculation of apparent dissociation constants for the metal ions (Figure 3 and Table 1). A two-site binding model was required to fit the experimental data obtained with 2AP54, whereas a one-site model was sufficient to describe titrations of 2AP57. These findings suggest that 2AP54, which according to the three-dimensional structure is located between the metal sites Mn1 and Mn2, monitors binding of two cations. 2AP57 is in proximity of only one site (Mn1) and its response thus obeys a one-site binding model.

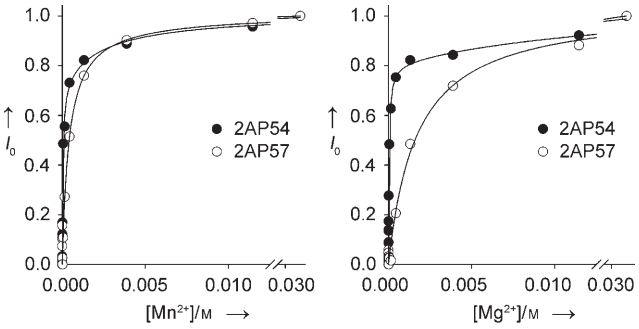

Figure 3. Fluorescence profiles for titrations of 2AP-labeled IIa-1 RNA (2AP54 and 2AP57) with $MnCl_2$ (left) and $MgCl_2$ (right). Normalized fluorescence intensity (I_0) is plotted versus metal-ion concentration. Lines represent fits of the experimental data with one-site (2AP57) and two-site (2AP54) binding models.

Table 1: Dissociation constants (K_d) for the binding of metal ions to 2AP-labeled IIa-1 RNA.[a]

		2AP54	2AP57
Mn^{2+}	K_d1	$3.9 \pm 2.1 \times 10^{-5}$	$4.2 \pm 2.2 \times 10^{-4}$
	K_d2	$2.5 \pm 1.0 \times 10^{-3}$	–
Mg^{2+}	K_d1	$3.7 \pm 2.0 \times 10^{-5}$	$1.7 \pm 0.9 \times 10^{-3}$
	K_d2	$1.8 \pm 0.9 \times 10^{-2}$	–

[a] K_d values (M) were derived from the fitting of one- and two-binding site models to the fluorescence titration data shown in Figure 3. Error ranges indicate 95% confidence intervals of fits. See Supporting Information for binding-curve equations.

Dissociation constants calculated from the titration data for 2AP54 and 2AP57 (Table 1) are in excellent agreement with the affinities of Mg^{2+} observed for, respectively, "strong" and "weak" binding sites in tRNA.[23] The measured affinities suggest that both sites represent location-specific chelated cations that are intrinsic elements of the IIa-1 RNA architecture.[16,24] Correlation of the fluorescence data with the crystal structure suggests that Mn1 represents the strong site, whereas Mn2 is a weak binding site. For Mg^{2+}, binding to site 1 in the 2AP-57-labeled RNA is about 490-fold tighter than to site 2. The affinity difference for Mn^{2+} is 63-fold. Both metal ions bind with about the same affinity to site 1. The more pronounced selectivity of site 1 for Mg^{2+} compared with Mn^{2+} is likely to be related to the strong preference of Mg^{2+} for hard oxygen ligands (such as the O2 atom of C55 in site Mn1) over soft ligands (such as the N7 atom of G52 in site Mn2).[23] Mn^{2+}, on the other hand, with its higher polarizability and d electrons involved in coordination, shows lower discrimination between sites involving O or N nucleophiles for coordination.[16]

The affinity of divalent metal ions for site 1 is reduced by at least one order of magnitude for 2AP57 compared with 2AP54 IIa-1 RNA. The crystal structure shows that replacement of adenine with 2AP at position 57 disrupts one of the hydrogen bonds that stabilizes C55, which acts as a direct ligand to metals bound at site Mn1 (Figure 2). The resulting higher conformational mobility of C55 likely leads to the observed weakening of metal-ion binding at that site.

Our crystallographic and solution studies of metal-ion binding to the HCV IRES IIa subdomain show that the functional architecture of this RNA depends on the presence of two divalent metal ions that stabilize a right-angled bend at the intersection of two helices. Structure-guided labeling of the RNA with the fluorescent base analogue 2AP allowed the correlation of Mn^{2+} and Mg^{2+} ion sites observed in the crystal with the binding of divalent metal ions in solution. As the bent architecture of the IIa subdomain is required for the precise positioning of the IIb hairpin at the 40S ribosomal subunit,[6,7] the divalent metal ions bound at the internal bulge of IIa are biologically relevant, intrinsic structural elements of the IRES RNA fold. Consequently, interference with the divalent metal ion core of the subdomain IIa bulge, for example, by binding of a specific ligand, may provide an approach to inhibit translation of the viral RNA. The presence of two closely spaced architectural metal ion sites within the highly organized IIa bulge might facilitate the structure-guided discovery of ligands that bind specifically to the IIa subdomain while displacing the cations by exploiting structural electrostatic complementarity.[25]

Received: September 15, 2006
Published online: November 28, 2006

Keywords: fluorescent probes · hepatitis C virus · molecular recognition · RNA structures · X-ray diffraction

[1] T. V. Pestova, V. G. Kolupaeva, I. B. Lomakin, E. V. Pilipenko, I. N. Shatsky, V. I. Agol, C. U. Hellen, *Proc. Natl. Acad. Sci. USA* **2001**, *98*, 7029.
[2] G. A. Otto, J. D. Puglisi, *Cell* **2004**, *119*, 369.
[3] H. Ji, C. S. Fraser, Y. Yu, J. Leary, J. A. Doudna, *Proc. Natl. Acad. Sci. USA* **2004**, *101*, 16990.
[4] E. A. Brown, H. Zhang, L. H. Ping, S. M. Lemon, *Nucleic Acids Res.* **1992**, *20*, 5041.
[5] J. S. Kieft, K. Zhou, R. Jubin, M. G. Murray, J. Y. Lau, J. A. Doudna, *J. Mol. Biol.* **1999**, *292*, 513.
[6] C. M. Spahn, J. S. Kieft, R. A. Grassucci, P. A. Penczek, K. Zhou, J. A. Doudna, J. Frank, *Science* **2001**, *291*, 1959.
[7] D. Boehringer, R. Thermann, A. Ostareck-Lederer, J. D. Lewis, H. Stark, *Structure* **2005**, *13*, 1695.
[8] P. J. Lukavsky, I. Kim, G. A. Otto, J. D. Puglisi, *Nat. Struct. Biol.* **2003**, *10*, 1033.
[9] A. J. Collier, J. Gallego, R. Klinck, P. T. Cole, S. J. Harris, G. P. Harrison, F. Aboul-Ela, G. Varani, S. Walker, *Nat. Struct. Biol.* **2002**, *9*, 375.
[10] J. S. Kieft, K. Zhou, A. Grech, R. Jubin, J. A. Doudna, *Nat. Struct. Biol.* **2002**, *9*, 370.
[11] R. Klinck, E. Westhof, S. Walker, M. Afshar, A. Collier, F. Aboul-Ela, *RNA* **2000**, *6*, 1423.
[12] P. J. Lukavsky, G. A. Otto, A. M. Lancaster, P. Sarnow, J. D. Puglisi, *Nat. Struct. Biol.* **2000**, *7*, 1105.
[13] F. Odreman-Macchioli, F. E. Baralle, E. Buratti, *J. Biol. Chem.* **2001**, *276*, 41648.
[14] In the crystal, the overhanging residues 70 and 117 align in a coplanar orientation with the 3′-terminal bases in neighboring RNAs to form intermolecular Watson–Crick pairs.
[15] Attempts to crystallize the IIa-1 construct in the absence of divalent cations were unsuccessful. Crystals obtained in the presence of magnesium only (no manganese present) yielded a three-dimensional structure that was essentially identical to the Mg^{2+}/Mn^{2+} structure, albeit at inferior resolution.
[16] D. E. Draper, *RNA* **2004**, *10*, 335.
[17] E. Ennifar, P. Walter, P. Dumas, *Nucleic Acids Res.* **2003**, *31*, 2671.
[18] Five additional metal ion sites were identified at crystal packing interfaces of IIa-1 RNA molecules (Table S2 in the Supporting Information).
[19] S. M. Freier, M. Petersheim, D. R. Hickey, D. H. Turner, *J. Biomol. Struct. Dyn.* **1984**, *1*, 1229.
[20] N. G. Walter, D. A. Harris, M. J. Pereira, D. Rueda, *Biopolymers* **2001**, *61*, 224.
[21] S. Shandrick, Q. Zhao, Q. Han, B. K. Ayida, M. Takahashi, G. C. Winters, K. B. Simonsen, D. Vourloumis, T. Hermann, *Angew. Chem.* **2004**, *116*, 3239; *Angew. Chem. Int. Ed.* **2004**, *43*, 3177.
[22] M. Kaul, D. S. Pilch, *Biochemistry* **2002**, *41*, 7695.
[23] T. Pan, D. M. Long, O. C. Uhlenbeck, *The RNA World* (Eds.: R. F. Gesteland, J. F. Atkins), CSHL, Cold Spring Harbor, NY, **1993**, p. 271.
[24] T. Hermann, E. Westhof, *Structure* **1998**, *6*, 1303.
[25] T. Hermann, *Angew. Chem.* **2000**, *112*, 1962; *Angew. Chem. Int. Ed.* **2000**, *39*, 1890.

